ACS NANO

ARTICLE

Filtration Efficiencies of Nanoscale Aerosol by Cloth Mask Materials Used to Slow the Spread of SARS-CoV-2

Christopher D. Zangmeister,* James G. Radney, Edward P. Vicenzi,§ and Jamie L. Weaver§

Cite This: *ACS Nano* 2020, 14, 9188–9200

Read Online

ACCESS | Metrics & More | Article Recommendations | SI Supporting Information

ABSTRACT: Filtration efficiency (*FE*), differential pressure (Δ*P*), quality factor (*QF*), and construction parameters were measured for 32 cloth materials (14 cotton, 1 wool, 9 synthetic, 4 synthetic blends, and 4 synthetic/cotton blends) used in cloth masks intended for protection from the SARS-CoV-2 virus (diameter 100 ± 10 nm). Seven polypropylene-based fiber filter materials were also measured including surgical masks and N95 respirators. Additional measurements were performed on both multilayered and mixed-material samples of natural, synthetic, or natural-synthetic blends to mimic cloth mask construction methods. Materials were microimaged and tested against size selected NaCl aerosol with particle mobility diameters between 50 and 825 nm. Three of the top five best performing samples were woven 100% cotton with high to moderate yarn counts, and the other two were woven synthetics of moderate yarn counts. In contrast to recently published studies, samples utilizing mixed materials did not exhibit a significant difference in the measured *FE* when compared to the product of the individual *FE* for the components. The *FE* and Δ*P* increased monotonically with the number of cloth layers for a lightweight flannel, suggesting that multilayered cloth masks may offer increased protection from nanometer-sized aerosol with a maximum *FE* dictated by breathability (i.e., Δ*P*).

KEYWORDS: SARS-CoV-2, COVID-19, cloth masks, face masks, personal protection, aerosols, respiratory protection
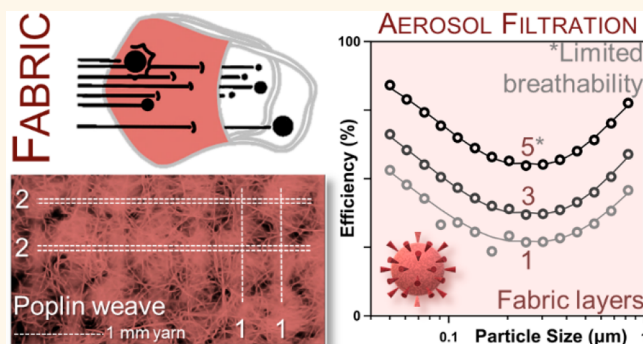
It has been recognized that the global spread of the Severe Acute Respiratory Syndrome Coronavirus 2 (SARS-CoV-2) has limited the supply of medical masks and particulate filtering facepiece respirators (e.g., N95), so it has been recommended that their use be restricted to healthcare settings.[1] As of this writing, the World Health Organization (WHO) and the United States Centers for Disease Control and Prevention (US CDC) suggest that cloth masks be used in nonmedical settings to reduce the transmission of SARS-CoV-2.[2,3] The majority of states in the United States and more than 130 nations, corresponding to over 75% of the global population, have issued official guidelines requiring or recommending the wearing of masks in public locations to mitigate the spread of COVID-19, the disease caused by SARS-CoV-2. Thus, nonmedical use of facial coverings will likely consist of masks made from a variety of fibrous cloth materials utilizing a range of designs and construction techniques. The WHO has stated the need for rapid dissemination of research investigating the performance of relevant mask parameters, for example, material, design, and construction, for reducing exposure to micrometer-sized droplets and nanometer-sized

aerosol particles at size ranges relevant to the virus (90 nm diameter core with ≈20 nm spike proteins).[1,3,4] Particle measurements from hosptials in Wuhan, China demonstrated that viable COVID-19 virus likely exists in particles with diameters between 250 nm and 500 nm.[5]

Facemasks can provide two modes of protection:[6] (1) by protecting the localized population from an infected mask wearer by trapping expelled virus-laden atomized material (droplets or aerosol) and (2) by protecting the mask wearer from ambient virus-laden atomized material by filtering inhaled air.[7] This reduces the risk of both direct and indirect viral exposure, respectively, thereby decreasing the probability of infection.[6]
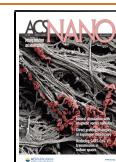
Prior research into cloth masks follows the history of infectious diseases spread by droplets or aerosol and dates back to the 1918−1919 influenza pandemic.[8,9] After that time, the publication record on the utility of cloth masks is sparse, and most research has focused on the effectiveness of single use masks available in many developed countries for healthcare or other occupational settings.[10−16] The prior research shows that cloth materials offer limited protection from particles in the size regime of SARS-COV2.[10−12]

When particles interact with a filter fiber, it is generally accepted that they are "collected" by a fiber and retained through van Der Waals forces.[17] For small particles, Brownian motion increases the probability a particle will interact with a filter fiber. At larger sizes, particles can be intercepted by a fiber when they are within one particle radius. When particle inertia becomes sufficiently high, the particle may no longer follow a flowing gas streamline resulting in a higher probability of inertially impacting a fiber. Electrostatic deposition, occurring due to a charge difference between a fiber and a particle, can also be important in some materials. Collectively, the sum of these efficiencies, diffusion (E_D), interception (E_R), impaction (E_I), and electrostatic deposition (E_B), yield the single fiber efficiency ($E_F = E_D + E_R + E_I + E_B$). The reader is directed to the seminal works by Brown,[18] Emi,[19] Fuchs,[20,21] and Liu[22] for detailed descriptions of filtration theory.

The filtration efficiency (FE) is a common metric for reporting particle capture efficiency of material and is related to E_F through[18−23]

$$FE = 1 - \exp\left(\frac{-4E_F\alpha L}{\pi D_f}\right) = 1 - \frac{N_D}{N_U} \tag{1}$$

where α, L, and D_f are the material porosity (i.e., packing density), filter thickness, and fiber or yarn diameter, respectively. The FE can be quantified by measuring the upstream and downstream (N_U and N_D, respectively) number density of particles per volume of air (particles cm^{-3}) where particles N_D passed through the filter and particles N_U were incident on the filter (see Figure S1 of the Supporting Information), and the difference between N_U and N_D represents the particles captured by the filter. FE is reported as a percentage (by multiplying eq 1 by 100) and is a function of the particle diameter (D), the flow rate through the filter, and the filter medium.[10−16,24,25]

The variability of test methods (mask materials vs fitted mask on human-scale forms vs standard mask testbed measurements) and the broad range of materials tested make direct quantitative comparability between published studies highly challenging.[10−16] In studies before 2020, the published FE of cotton-based fabrics was 5% to 60% when tested against an NaCl aerosol with 20 nm ≤ D ≤ 1000 nm, 10% for spherical 100 nm latex particles, and <10% for 100 nm diesel soot.[10−12] Generally, the published FE of cloth filter media is much lower when compared to facepiece respirators that are regulated for use in healthcare and other professional settings; for example, the FFP2 (EU standard, EN 149−2001) or the N95 (USA, NIOSH-42C FR84), which are rigorously tested to ensure FE ≥ 94% and FE ≥ 95%, respectively, for 300 nm D NaCl.[26,27] Notably, a recently published study suggests that masks from cloth filter media can be constructed that may afford better protection for the wearer than an N95 respirator for particles between 10 nm and 200 nm in size due to an

enhancement in E_B by specific types of cloth arranged in a multilayered configuration.[15]

The study reported here aims to aid in the call for research testing the performance of cloth-based media that are relevant for mask use.[3] The FE and differential pressure (ΔP, Pa), which is related to breathability, were measured for 32 relevant cloth materials (14 cotton, 1 wool, 9 synthetic, 4 synthetic blends, and 4 synthetic/cotton blends) that may be used in facemasks. The FE and ΔP were measured under controlled laboratory conditions utilizing size selected NaCl aerosol with particle mobility diameters (D_m) between 50 and 825 nm, a size regime relevant for the removal of SARS-CoV-2 particles,[6,28] and in accordance to standard established filter testing protocols, Parts 3 and 5 of EN 1822 and ISO 29463, using size selected charged and neutralized aerosol, respectively. For comparison, the FE and ΔP of 7 polypropylene containing materials (2 surgical facemasks, an N95 filter, N95 fabric, a high- and low-density medical wrap, and a purported HEPA vacuum bag), 2 papers (coffee filter and paper towels), and 4-layered samples of different materials were also measured. The samples in this study were systematically chosen and characterized by their composition, yarn count, weave type (which has been relatively understudied),[29] and mass with the goal of establishing a relationship between these parameters and measured FE and ΔP when tested against nanometer-sized aerosol under well controlled laboratory conditions using established filter testing protocols.

RESULTS AND DISCUSSION

Both nanometer-sized aerosol particles and micrometer-sized droplets can be captured by a filter.[17] The FE is a function of D_m, D_f, fiber packing density, and flow rate.[25] Freshly generated particles may be highly charged but immediately start to neutralize after emission.[30] Ambient aerosols are expected to have a net neutral average charge that follows a Boltzmann distribution after <100 min aloft[25] (note, lifetimes of nanoparticles span hours to days over this size range).[31] Differences in the charge state or distribution of charges of the aerosol may impact the measured FE with E_B typically enhancing FE.[32]

The distribution of particle sizes filtered by a material can be broadened by using random arrays or layered structures containing a distribution of fiber diameters.[23,33] This has allowed for the development of filtration media with excellent FE across a broad range of D_m at reasonable ΔP (e.g., the N95 mask and HEPA filters, see Figure 1B$_{1,2}$) and may also give insight into the design and use of cloth materials for facemasks for the capture of virus-laden aerosols. Therefore, an understanding of the filter structure (including weave structure, yarn count, and yarn mass) and material composition (natural, synthetic, or blended materials) may be important for the FE of cloth materials and may provide a deeper understanding in the complex parameter space that influences the FE of cloth mask materials.

There have been several suggestions that FE may be related to textile parameters. Recently, Konda et al. (2020)[15] indicated an increase in FE as a function of higher yarn count (described as TPI in the cited article and summarized in their Figure 3, and which herein will be discussed as yarns inch^{-2} unless otherwise noted; 2.54 cm = 1 in). Other studies have suggested that the cover factor, defined as the sum of the number of yarns per unit length to the square root of the yarn count for the warp and weft directions (see Supporting Information for
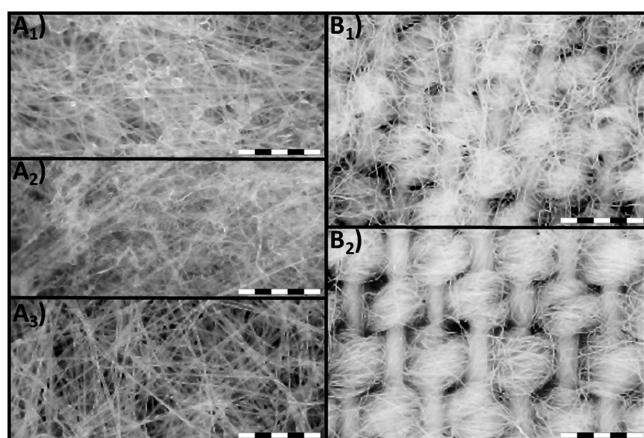
Figure 1. Transmitted light imagery of nonwoven and woven face mask materials. (A_{1-3}) Outer, intermediate, and inner layers of a N95 mask showing randomly oriented spun-bond (A_1) and melt-blown (A_2 and A_3) synthetic fibers.[34] ($B_{1,2}$) Outer and inner surfaces of poplin weave cotton fibers in lightweight flannel (sample Cotton 10). Note: Transmitted light grayscale intensities have been inverted so fibers appear lighter relative to voids; all scale bars represent 1 mm with subsections of 200 μm in length.

definitions), is also related to a fabric's filtration level (but not *FE* directly).[35] The cover factor indicates the extent to which the area of a fabric is covered by one set of yarns, and a fabric with a high cover factor would have a low density of open space relative to fabric material for a given area. Cover factor is differentiated from packing density, as cover factor assumes the yarns are solid and nonporous, thus underestimating a materials porosity. Other parameters that may play a role are yarn mass, fabric texture, and fabric composition. Past studies at the National Bureau of Standards (NBS, currently the National Institute of Standards and Technology, NIST) indicated relationships between yarn count, fabric mass, and weave type with permeability to air, which is related to the ΔP and the level of breathability through the material.[29]

Electrostatics, as discussed by Konda et al. (2020)[15] and Zhao et al. (2020),[36] may be another important parameter and are addressed in this investigation by studying the impact of particle and cloth charge (see further). A theoretical model of fabric electrostatics was proposed by Alekseeva et al. (2007)[37] and suggested that fabrics can behave like a capacitor, collecting electric charge in the gaps (pores) in fibers of the fabric. The specific properties are potentially dependent on fiber composition, weave type and tightness (related to cover factor), production and processing methods, and can be influenced by atmospheric conditions (humidity, pressure, and temperature).[38] The electrostatics of cloth materials are more commonly (although not always) discussed for synthetic as opposed to natural fibers.[39]

The *FE* values of 41 samples, 32 cloth materials (14 cotton, 1 wool, 9 synthetic, 4 synthetic blends, 4 synthetic/cotton blends), 2 paper materials, and 7 polypropylene-based fiber filter materials, were measured at 15 equally log-spaced mobility diameters (D_m) resulting in D_m spanning 50 nm $\leq D_m \leq$ 825 nm. Particles were charge neutralized (as recommended by Parts 3 and 5 of the EN 1822 mask filtration protocol) using a soft X-ray source and size selected by a differential mobility analyzer.[27] For comparison, seven of the samples were reneutralized after size selection in accordance with the ISO 29643 filter testing standard. Particle number

densities upstream (N_U) and downstream (N_D) of the sample were recorded by condensation particle counters (CPC) for 30 s at 1 Hz at each D_m. These data were averaged, and 1σ standard deviations were calculated at each D_m bin. Measured 1σ standard deviations in N were $\approx$2.5% with a CPC accuracy of $\approx$3% for $N < 2 \times 10^4$ cm^{-3} (independently calibrated by optical methods),[40] and $\approx$2% day-to-day variability in *FE* for the same sample and $\sim$1% sample-to-sample variability in *FE*, resulting in an assumed 5% combined uncertainty for *FE*; see Figures S13 and S28 for day-to-day and sample-to-sample variabilities, respectively. The N_D was scaled based upon the CPC counting mode (single particle versus photometric; see Figure S2 and corresponding discussion in the Supporting Information), and the *FE* was calculated from eq 1.

Representative *FE* values as a function of D_m are shown in Figure 2 for four of the tested samples (an N95 respirator, the
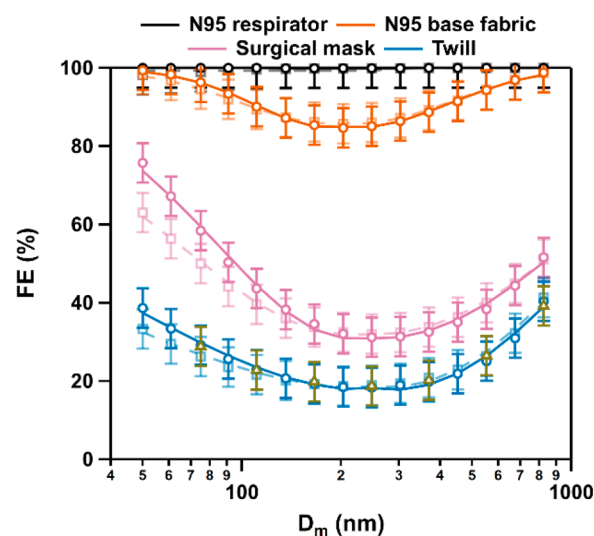

Figure 2. Measured filtration efficiency (*FE*) as a function of particle mobility diameter (D_m) for an N95 respirator (black), the N95 base fabric (orange), a surgical mask (pink), and a twill (blue). The solid bold lines and circles represent the base sample, while the dashed light lines and squares correspond to the reneutralized samples. Olive triangles correspond to the twill *FE* measured with an aerosol particle mass analyzer and reneutralization. Uncertainties in FE are ±5%. See discussion in text. Corresponding distributions of N_U and N_D can be found in Section S3 of the Supporting Information.

base fabric that is used to make an N95 respirator, a surgical mask, and a 65%/35% cotton/polyester twill polyester/cotton blend 3, twill weave, 229 yarns inch^{-2}). Importantly, the measured data capture the *FE* under conditions where leaks are absent. The aerosol after size selection had moderate net charge (q, where $+1 \leq q \leq \sim + 4$ due to charge neutralization prior to the measurement).[41] The impact of particle charge on *FE* was tested by also measuring the *FE* of 7 samples that were reneutralized after size selection (dashed light lines and squares in Figure 2 and blue traces in Figures S21, S36, S39, S49, S50, S51, and S52). The measured data indicate that particle charge does not impact *FE* of the measured cloth materials. In addition, the *FE* of polyester/cotton blend 3 was quantified by passing the size selected aerosol through an aerosol particle mass analyzer (APM) and subsequently reneutralizing (olive triangles in Figures 2 and S39). The tandem DMA-APM effectively removes the presence of particles with $q > + 1$ that
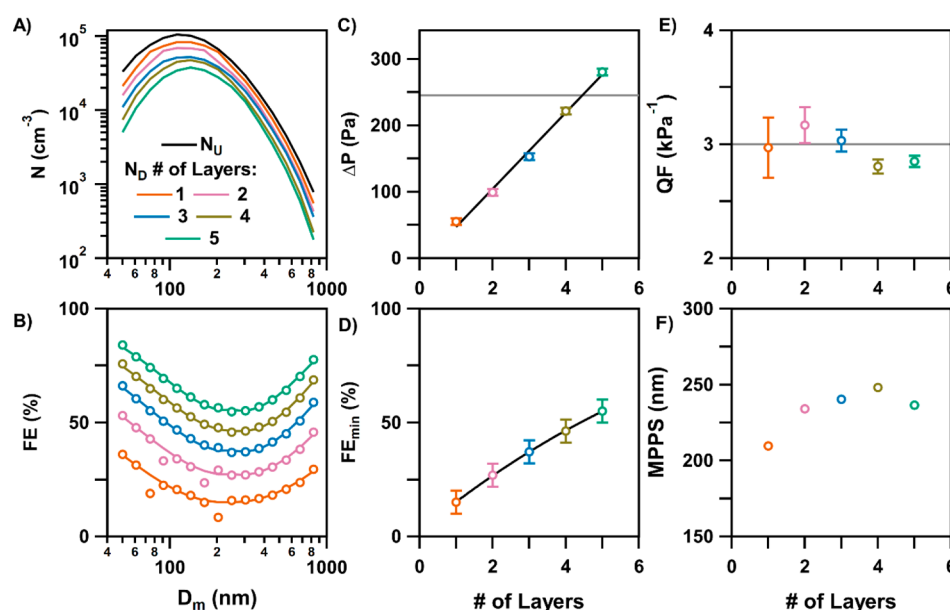
Figure 3. Filtration efficiency (*FE*) as a function of number of fabric layers for a cotton fiber poplin weave in a lightweight flannel (Cotton 10). (A) Particle number densities per volume of air for the upstream (N_U, black) and downstream (N_D) particle counters as a function of number of layers (colored lines). Shown N_U was measured for a one-layer sample but was representative of the N_U measured for all samples. (B) Calculated *FE* as a function of D_m and number of layers (colored lines). (C) Measured differential pressure (Δ*P*, Pa) across the material as a function of number of fabric layers. Gray line and plot maximum correspond to NIOSH recommended maximum differential pressure across filter mask for exhaling (245.2 Pa, 25 mm H_2O) and inhaling (343.25 Pa, 35 mm H_2O), respectively.[27,45] (D) Minimum measured FE_{min} as a function of number of layers. (E) Quality factor (*QF*) as a function of number of fabric layers. Horizontal line shows *QF* = 3 (WHO recommendation).[3] (F) Maximum penetrating particle size (*MPPS*, nm) as a function of number of fabric layers. Lines in B correspond to bi-Gaussian fits of the data, while lines in C and D are shown to guide the eye.

may exit the DMA.[42,43] With the exception of the surgical mask that uses polypropylene layers for filtration, aerosol reneutralization (and mass selection) did not affect *FE* (all values were within 1σ uncertainty), see Figure 2, suggesting that E_B is not significant for these cloth materials under current conditions and is in agreement with previous observations.[10]

The *FE* values presented here are likely higher than typically measured on a mask testing device as required for regulatory compliance (*e.g.*, US 42 CFR 84 or EN143) and should be interpreted as the maximum expected *FE* of the material for mechanical processes (E_D, E_R, and E_I). Unless otherwise noted, the reported values are shown for aerosols that were not reneutralized after size selection (see additional sample *FE* curves of reneutralized aerosol in Section S3 of the Supporting Information).

Previous studies have reported values of FE_{min} and the most penetrating particle size (*MPPS*, *i.e.*, D_m at FE_{min}) for mask comparability.[10−16] In this study, FE_{min} and *MPPS* were determined by converting *FE* to penetration efficiency (*PE* = 100% − *FE*) and fit to a logarithmic bi-Gaussian distribution (see eq 2).[44] A bi-Gaussian distribution was chosen as it describes the shape of the data over the measured range and is loosely related to the functional form of *FE vs* D_m (see eq 1). The interpolated bi-Gaussian fits are shown for all measured samples in Section S3 of the Supporting Information with representative data in Figure 2.

An N95 mask is constructed of a multilayered assemblage of polymer fibers with a distribution of D_f to efficiently bind particles of all D_m resulting in *FE* values that are nearly invariant with D_m with an average *FE* of (99.9 ± 0.1)% (1σ standard deviation across the 15 measured D_m; see Figures 2 and S50). Except for the sample cut from a N95 mask, the *FE*

of each tested material had a consistent and typical U-shaped curve (increased inertial impaction and interception with larger D_m *vs* increased diffusion at smaller D_m),[25] see Figure 2, that was exclusive for each material tested (see Section S3 of the Supporting Information for all *N* and *FE vs* D_m plots). Some materials, for example, sueded polyester (Polyester 3, poplin weave, 152 yarns inch^{-2}), had a high *FE* (75%) at D_m < 200 nm and low *FE* (<25%) at D_m > 500 nm. In comparison, a heavy chiffon (Polyester 4, plain weave, 152 yarns inch^{-2}), exhibited a *FE* that was only weakly dependent on D_m, but averaged ∼30% across the entire D_m range. A third poplin weave, light chiffon polyester (Polyester 6) of the same yarn count and base-fiber of the previous two fabrics mentioned had an *FE* < 25% across the range of D_m sizes measured. All three have different areal masses (85 mg inch^{-2}, 107 mg inch^{-2}, and 38 mg inch^{-2}, respectively). These data suggest that *FE* has a complex interplay between fiber type, sample mass, and construction methods (weave or bond structures). A detailed correlation analysis of these parameters for several of the woven samples is discussed further.

Initial investigations of the efficacy of cloth masks during the 1918 influenza pandemic showed that increasing the number of cloth layers in a facemask (1 layer to 8 layers) was important in the reduction of microbial growth on plates placed downstream of fabrics and exposed to aqueous aerosol droplets containing bacteria.[8,9] Another study showed an analogous benefit by increasing the number of mask layers up to 4 layers of cotton gauze.[9] A similar trend was observed in this study for a lightweight flannel (Cotton 10) using 1 to 5 layers of cloth (see Figure 3). Figure 3A and B show *N* (particle concentration, particles cm^{-3}) and *FE* as a function of the number of layers, respectively. The Δ*P* (see Section S1, Figure
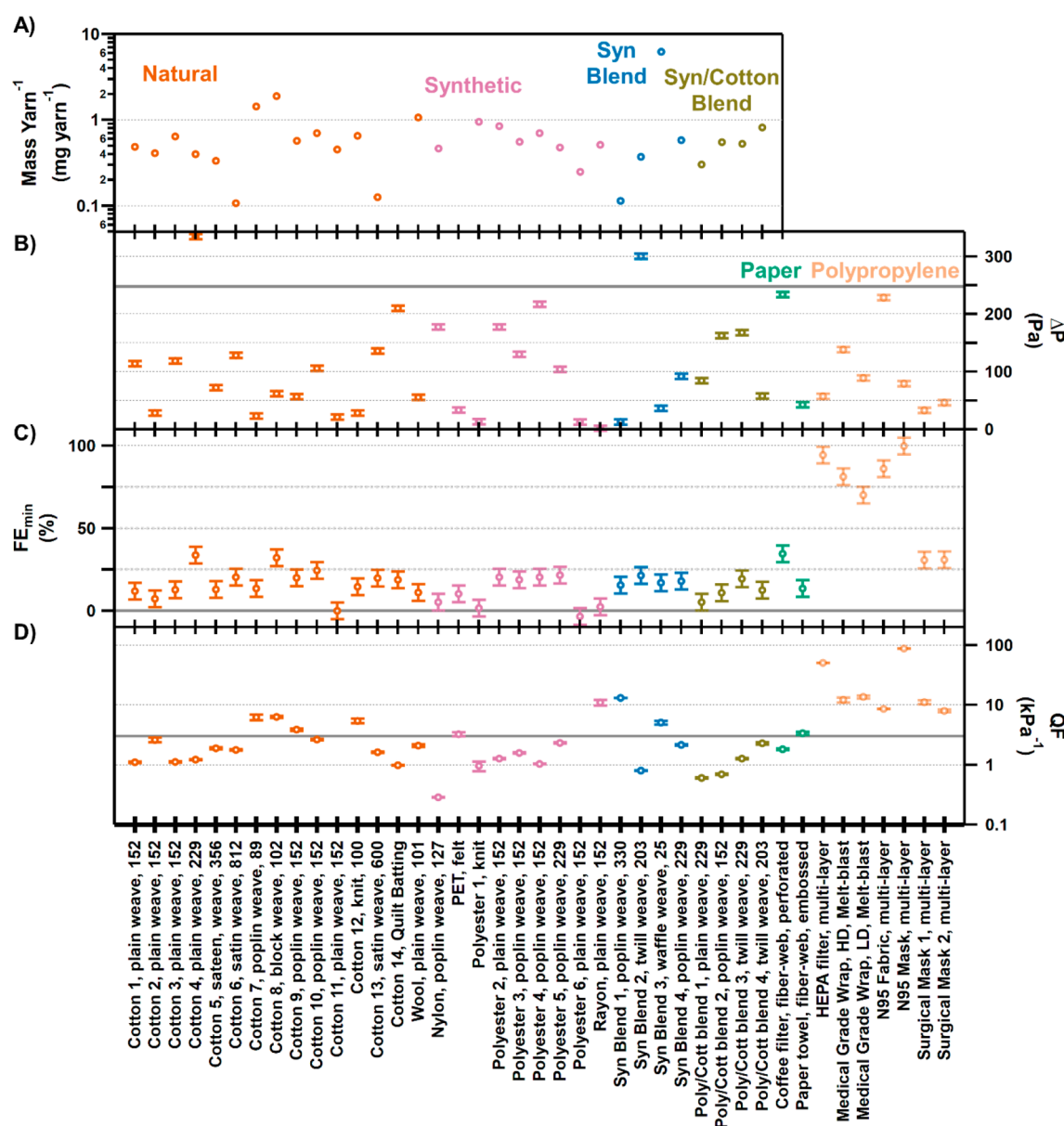
Figure 4. Measured samples categorized by type from left to right: cotton (orange), synthetic (pink), synthetic blend (blue), synthetic/cotton blend (olive), paper (green), and polypropylene-based (light orange). (A) Yarn mass (mg yarn^{-1}), (B) differential pressure across sample (ΔP, Pa), (C) minimum filtration efficiency (FE_{min}, %), (D) quality factor, QF (kPa^{-1}). The average most penetrating particle size (D_m) across all samples was 252 ± 45 nm with individual values plotted in Figure S5. Uncertainties in B and C are ±4.9 Pa ($2\times$ manometer read uncertainty) and $\pm5\%$ (expanded uncertainty), while uncertainties in D were propagated from B and C. Abbreviations: Polyester (poly) and Cotton (Cott).

S1) across the fabric and FE_{min} increase monotonically with the number of layers present (see Figure 3C,D). More than 4 layers of this sample exceeded the NIOSH recommended ΔP during exhalation through a fitted mask (245.2 Pa, 25 mm H$_2$O).[46] The quality factor (QF) was also calculated as a function of the number of layers, see Figure 3E. The QF is a commonly used factor to evaluate filter performance under common experimental conditions:[23]

$$QF = \frac{-\ln(1 - FE_{min}/100)}{\Delta P} \qquad (2)$$

QF increases as FE increases or ΔP decreases. QFs reported in the literature utilize both ln and log$_{10}$.[23,36,47] The ln form was used in this study in accordance with the WHO recom-

mendation.[3] The QF was nearly invariant with the number of fabric layers, consistent with multiplicative FE_{min} and additive changes in ΔP with the number of fabric layers. Lastly, the maximum penetrating particle size ($MPPS$), defined as the D_m of FE_{min}, shown in Figure 3F, is 300 nm for a single layer and slightly increases with the number of fabric layers to 350 nm for 4 layers of fabric.

The ΔP and FE curves were measured for 38 cloth materials spanning 50 nm $\leq D_m \leq$ 825 nm. The FE_{min} and $MPPS$ were calculated by fitting the distribution to a bi-Gaussian from which QF was determined (see Figure 4 for FE_{min} and QF and Figure S3 for $MPPS$; average $MPPS$ across all samples was (252 $\pm$ 45) nm). The samples, listed above and in Tables S1 and S2 in Section S2 of the Supporting Information, were classified by fiber content as natural, synthetic, synthetic blend, synthetic/

cotton blend, paper, and polypropylene-based. The ΔP and FE of the cloth and paper samples were measured utilizing two layers of the respective materials and as envisioned when constructing a multilayer mask. Synthetic blend 3 (waffle weave, towel) and medical-grade materials (high-density and low-density wraps, HD and LD, respectively) were measured as a single layer due to sample thickness (Synthetic blend 3) or per the manufacturer's use instructions (wraps). The N95, N95 fabric, and HEPA vacuum bag were constructed of multiple, separable thin layers of synthetic fibers and used as received. As of this writing, the medical-grade wraps are regulated for specific use in healthcare settings and are not currently approved for use in masks in the United States.[48] However, they have been utilized in emergency situations by frontline healthcare workers in the United States and are included only to aid in comparability to cloth and other tested materials. Additionally, while the HEPA vacuum bag tested here contains polypropylene, some HEPA filters may be made from inorganic glasses.

The areal mass yarn^{-1} (see Figure 4A), a normalized mass value and not an absolute value for each yarn set, spanned almost an order of magnitude across the range of cotton and synthetic samples. The measured ΔP (shown in Figure 4B) also spanned a broad range and was nearly zero for open weaves, for example, Cotton 11 (muslin cotton) and Rayon, and near 334 Pa (34 mm H_2O) for the most tightly woven samples (e.g., Cotton 4, down proof ticking), which also was one of the highest yarn count samples measured. The FE of the measured samples ranged from $\approx$100% for a cut-out section from an N95 mask to 0% (within measurement uncertainty) for Polyester 6 (light chiffon) and Cotton 11 (muslin). Porosity, which was reported for the fabrics measured by Konda *et al.* (2020),[15] was not calculated for these samples as the length scale of smaller fabric pores (>150 nm) was below the resolution of the imaging instrument ($\approx$ 20 μm, see Figure S4, Figures S54, and S55).

Of the fabrics tested, the top three fabrics with the highest FE_{min} were 100% cotton: Cotton 4 (down proof ticking), Cotton 8 (woven hand towel), and Cotton 10 (lightweight flannel). The FE_{min} of Cottons 4 and 8 did not exhibit a statistically significant difference ($p > 0.05$), assuming 5% uncertainty. Cotton 4 (229 yarns inch^{-2}) exceeded the NIOSH exhalation ΔP limit (245 Pa, 25 mm H_2O).[46] Notably, it approached the maximum 343 Pa (35 mm H_2O) inhalation ΔP limit recommended for mask use by NIOSH.[27] For comparability of cloth to other tested materials, the measured FE_{min} of 2 layers of a high performing cloth (Cotton 8, FE_{min} = 32%) was lower than those measured for the low- (FE_{min} = 70%) and high-density (FE_{min} = 86%) medical-grade wraps, the N95 mask (FE_{min} > 99.9%), and the HEPA vacuum bag (FE_{min} = 94%). Cotton 8 also had a similar FE_{min} to the two tested surgical masks (30.5%) and coffee filter (34.4%). The other top cotton fabrics were of average ($\approx$ 150 yarns inch^{-2}) to low ($\leq$100 yarns inch^{-2}) yarn counts, with the lowest being Cotton 8 ($\approx$ 100 yarns inch^{-2}). These materials had 24% $\leq$ FE_{min} $\leq$ 32%, and 57 Pa (5.8 mm H_2O) $\leq$ ΔP $\leq$ 106 Pa (10.8 mm H_2O).

The other two fabrics in the top five were Synthetic blend 2 (twill weave, synthetic, $\approx$ 200 yarns inch^{-2}) and Polyester 5 (100% polyester, poplin weave, $\approx$ 230 yarns inch^{-2}). The FE_{min} performances of these two fabrics do not exhibit a statistically significant difference (see Table S2 in Section S1 in the Supporting Information) assuming an uncertainty of 5%. The

synthetic blend had a moderately high yarn count and the second highest ΔP (300 Pa, 30.6 mm H_2O) of the all samples. While it met the NIOSH inhalation ΔP limit,[45] it exceeded the exhalation limit.[46] Polyester 5 had a higher yarn count, and the ΔP (104 Pa, 10.6 mm H_2O) was well below NIOSH limits. No trends were observed between the type of fabric weave and the measured FE_{min}. The top five fabrics had weaves ranging from plain (Cotton 4), to block (Cotton 8), to poplin (Cotton 10, Polyester 5) and twill (Synthetic blend 2). Descriptions of weaves can be found in Table S38.

Visual inspection of all top performing, highest FE_{min}, cotton samples showed some amount of fiber raised from the weave structure. For Cotton 9, which fell within the top half of FE_{min} performance, and Cotton 10, the raised fibers were nap formed during manufacturing. Nap is an intentional textural feature made from directionally oriented raised fibers that protrude from the 2-dimensional plane of the fabric. Directionality can be lost without intervention (i.e., brushing) as the result of use, and the fibers can form aperiodic patterns similar to those seen in fiber-web fabrics (e.g., Figure 1). Imaging of the two flannels showed they were more heavily napped on their outer side as opposed to their inner side and were the most heavily napped/raised fiber textured of almost all the materials measured (see Figures S15 and S17 in Section S3 of the Supporting Information for imaging of each measured sample and Figure 1B$_{1,2}$). These two flannel, Cotton 10 and Cotton 9, had similar yarn counts ($\approx$ 150 yarns inch^{-2}) and yarn widths: Cotton 10 (*weft*) 0.26 mm $\pm$ 0.04 mm, (*warp*) 0.18 mm $\pm$ 0.03 mm; Cotton 9 (*warp*) 0.19 mm $\pm$ 0.02 mm, (*weft*) 0.30 mm $\pm$ 0.03 mm). The other top performing cotton fabrics exhibited a similar, raised fiber texture, although not to the same extent. This raised fiber texture was not observed for Polyester 5 or Synthetic blend 2. Additional textural features were observed as raised fibers for Cotton 8 (woven hand towel) and are likely related to fabric construction.

The fabric with the lowest FE_{min} was Polyester 6 (lightweight chiffon), followed by, in ascending FE_{min}, Cotton 11 (muslin), Polyester 1 (knit), Rayon, and (Polyester/cotton blend 1, 65% polyester/35% cotton). Four out of the five fabrics with the lowest FE_{min} were synthetic. Two fabrics, Polyester 6 and Cotton 11, had visually open weave structures compared to all other fabrics analyzed (see Figures S19 and S29 in Section S3 of the Supporting Information). All had yarn counts <250 yarns inch^{-2}. Rayon, Polyester 1, and Polyester 6 had no apparent raised fibers, while Polyester/cotton blend 1 and Cotton 11 had very few observable raised fibers. All were highly breathable, with ΔP < 88.2 Pa (9 mm H_2O).

The QF is a relative metric for assessing the overall performance of a filter through the combination of FE_{min} and ΔP (see eq 2 and Figure 4D). For measurements at similar flow rates, higher QF typically implies improved performance; the WHO recommends utilizing cloth masks with QF > 3.[3] QF ranged from >50 kPa^{-1} for the N95 mask and HEPA filter to <0.3 kPa^{-1} for Nylon, Cotton 11 (muslin), and Polyester 6 (lightweight chiffon). Paradoxically, two of the highest QFs were for materials with low FE_{min} and ΔP: Rayon, QF = (10.8 $\pm$ 2.5) kPa^{-1}, FE_{min} = 2.1%, and ΔP = 1.9 Pa, and Synthetic blend 1, cotton/Spandex, (13.5 $\pm$ 2.5) kPa^{-1}, 15.3%, 13 Pa. These QF values are similar to those of the medical grade wraps (QF $\approx$ 13), surgical masks (average QF $\approx$ 9), and the N95 fabric (QF $\approx$ 8), which all had significantly higher FE_{min}. For these low ΔP materials, FE_{min} can be improved by constructing masks with many layers (compared to the 2 layers
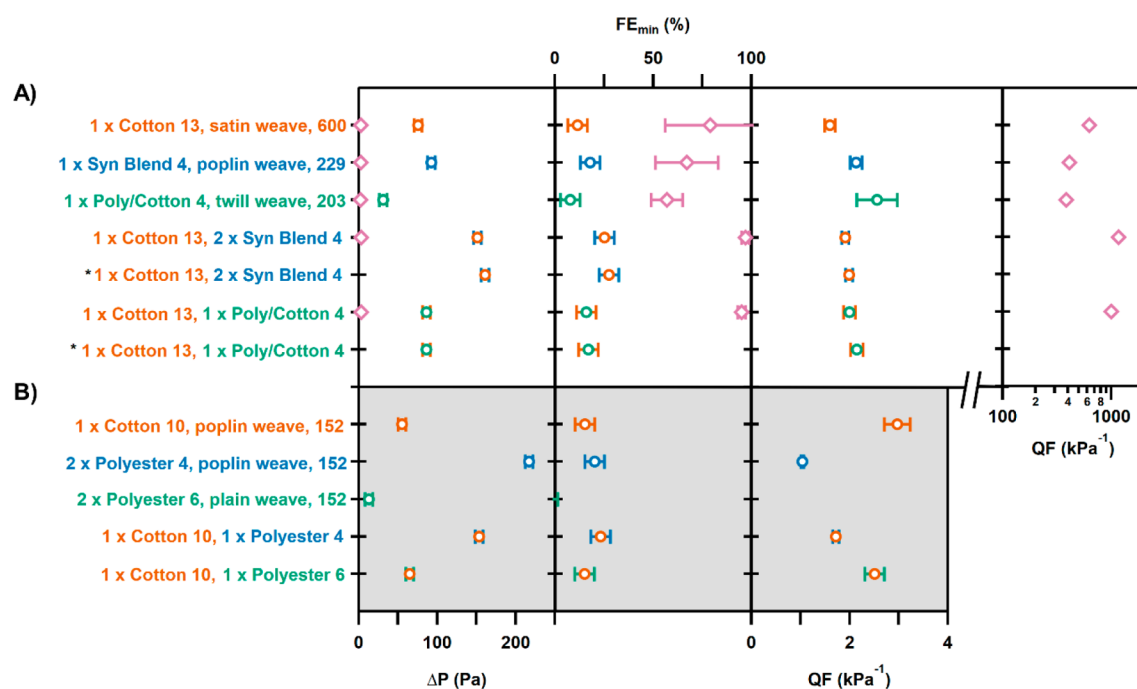
Figure 5. Comparison of ΔP, FE_{min}, and QF for single component layers and mixed layered materials. Samples and mixed samples are coordinated by color. (A) Top 3 samples are single layers and bottom 4 are mixtures using fabric samples either similar, or identical to those reported in Konda et al. (2020).[15] Samples marked with ∗ were rubbed together for 30 s while wearing latex gloves to aid in sample charging as in Zhao et al. (2020).[36] Pink diamonds show data from Konda et al. (2020).[15] (B) Top 3 samples are single layers and bottom 2 are mixtures using fabric samples exclusive to this investigation.

used presently) while maintaining QF (e.g., Figure 2E); however, the number of layers required to obtain the desired FE_{min} will likely limit functionality in other ways (e.g., $FE_{min} > 30\%$ would require ~34 layers of Rayon), whereas Cotton 8, woven hand towel, $(6.2\ kPa \pm 0.3)\ kPa^{-1}$, 32%, 62 Pa, had a moderate QF, FE_{min}, and ΔP, respectively.

The FE_{min} and ΔP data were statistically evaluated using correlation calculations to determine if relationships existed between measured values and textile parameters for both 100% cotton and 100% polyester fabrics. No statistically significant relationships were found for parameter sets with a sufficient number of samples ($n = 5$ for 100% polyester and $n = 11$ for 100% cotton). Details of analyses and results can be found in Tables S34−S37 in Section S5 of the Supporting Information. Sample sizes, after they were controlled for outliers and samples with easily discernible weave patterns and yarn counts, were relatively small ($2 < n > 9$) and may have attributed to the nonsignificant results. A larger data set from additional samples collected from similarly controlled populations may provide more insight into the effect of these variables on FE_{min} and ΔP.

In their recent paper, Zhao et al. (2020)[36] related the measured electrostatic properties of common household fabrics (many similar to those studied here) to the fiber chemistry. A similar discussion can be had relating the mechanical filtering ability of a textile to the fiber sources, yarn widths, and textile construction. Mechanical filtration of aerosols by fiber filters is partially dependent on the fiber diameter[49] and the range of diameters of the fibers.[50] Fiber shape may also be an important factor.[51] For synthetic-based apparel textiles, the fibers used to construct yarns tend to be set and have a relatively small variability in width and shape.[39] Generally, natural fibers have more variability, which can be

influenced by many factors. For plant-sourced materials (e.g., cotton), these factors can include plant type, growing conditions, and postharvesting processing methods.[52] Cotton has been reported to have fiber diameters from ≈1 μm to ≈22 μm with a similar range of fiber width variability (≈ 20 μm) found within singular crops. For animal-sourced materials (e.g., wool), factors may be animal type/breed[53] and seasonal nutrition levels of the animals.[54] Sheep wools have been reported to have fiber diameters spanning <17 μm to ~40 μm,[55] with intrabreed variability of ≈20 μm. Although this in range fiber diameter is not as broad as those reported for high filtering synthetic nanofibers (spanning nm to μm),[56] they do provide a broad fiber diameter range and can be used to form fiber-webs for particle filtration. These two features are those often found in filter media that have been shown to have good FE values.[57]

In this study, many woven fabrics were found to form fiber-webs, with the highest concentration being apparent for the 100% cotton flannel samples. These webs, the result of fibers being raised away from the woven structure of the textile, can result in an increase of material disorder, thereby disrupting flowing gas streamlines and providing more surfaces with which the aerosols can interact. This may provide a mechanism to explain why the medium range yarn count (≈ 150 yarns inch^{-2}) Cotton 10 out-performed other fabrics with higher yarn counts (e.g., Cotton 6 and Cotton 13) or synthetics with visually tighter weaves (e.g., Polyester 5). Additionally, this suggests that cover factor, discussed above, may not be a good individual indicator of FE for fabrics displaying these textures. Interestingly, the cotton batting sample (Cotton 14) showed a relatively low FE_{min} despite consisting of fiber-webs. More research is needed to understand these observations.
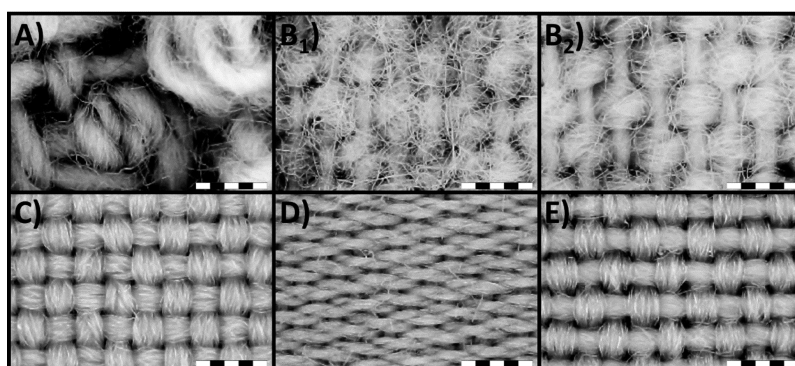
Figure 6. Transmitted light images of top performing fabrics based on FE_{min} and ΔP that fall within NIOSH guidelines and are listed in Table 1: (A) Cotton 8 (hand towel, 100% cotton, block weave), (B_1, B_2) outer and inner surfaces of Cotton 10 (light flannel, poplin weave, 100% cotton), respectively, (C) Polyester 5 (apparel fabric, poplin weave, 100% polyester), (D) Cotton 6 (inner surface, pillowcase, 100% cotton, satin weave, see SI for image of other side), and (E) Polyester 2 (soft spun, 100% polyester, plain weave). Note: Transmitted light grayscale intensities have been inverted so fibers appear lighter relative to voids; all scale bars represent 1 mm with subsections of 200 μm in length.

Table 1. Top Fabrics Based on FE_{min} that Fall within NIOSH ΔP Guidelines[a]

sample and weave	source/descriptor	TPI (yarn inch^{-2})	FE_{min} (%)	ΔP (Pa)	QF^c (kPa^{-1})
Cotton 8, block	hand towel	102[b]	32.0 ± 1.6	61.8 ± 4.9	6.25 ± 0.27
Cotton 10, poplin	lightweight flannel	152	24.3 ± 1.07	106.0 ± 4.9	2.62 ± 0.07
Polyester 5, poplin	poplin apparel fabric	229	21.4 ± 1.08	104.0 ± 4.9	2.32 ± 0.06
Cotton 6, satin	pillowcase	812	20.3 ± 1.02	128.5 ± 4.9	1.77 ± 0.04
Polyester 2, plain	soft spun apparel fabric	152	20.2 ± 1.02	177.6 ± 4.9	1.27 ± 0.03

[a]Samples and sources, yarns inch^{-2} (reported as threads inch^{-2} (TPI) in the table), FE_{min}, ΔP, and QF for 2 layers of select samples. Uncertainties are 1σ. [b]Sample is constructed of a complex design that results in a variable TPI across the fabric area. Reported value is an estimated average TPI. [c]The WHO recommends utilizing cloth masks with $QF > 3$.[3]

In addition to measuring materials from a single type of cloth, two-layered (multimaterial) structures were also investigated in accordance with recent findings by Konda *et al.* (2020)[15] who measured FE_{min} > 95% for masks comprised of combinations of two layers of a synthetic and natural fabric using NaCl aerosol that was not size selected. Combinations of cotton and synthetic fabrics identical, or nearly identical, to those outlined in Konda et al. were tested here, and the present results were not consistent with the prior findings (Figure 5A). Because of the low-pressure differentials measured, QF values in Konda et al. were over 1000 kPa^{-1}, 250−500-times higher than measured in this study; see values in Figure 5A.[15] Additional combinations that were exclusive to this investigation (see Figure 5B) were also tested. Konda *et al.* hypothesized that the measured FE_{min} resulted from dissimilar layered fabrics increasing electrostatic charge (and hence E_B) at the interface between the two layers. In this study, an attempt was also made to increase the charge between the layered structures by rubbing the materials against one another wearing latex gloves for 30 s, as described recently by Zhao et al. (2020)[36] and by Perumalraj (2015)[58] for woven fabrics. This did not significantly impact the measured FE_{min} (see Figure 5A). Subsequently, the multilayered samples also did not exhibit a significant difference in the measured FE_{min} when compared to the product of the individual FE_{min} for the components (sum of individual efficiencies in eq 1), see Figure 5A. Zhao et al. (2020)[36] showed that intense rubbing of materials using latex for 30 s increased the FE for some synthetics but did not increase FE for cotton samples. The high FE reported by Konda et al. (2020)[15] is an intriguing observation that is inconsistent with the results presented here and may be an artifact of sampling a freshly generated

NaCl aerosol (e.g., Forsyth et al. (1998))[59] that has not reached charge equilibrium (either through the passage of time or utilizing a charge neutralizer prior to exposing the aerosol to the sample). Thus, while their FE_{min} may be applicable to freshly emitted virus-laden particles (e.g., from a cough *etc.*), they are likely less representative of neutral or weakly charged particles or those that persist in the ambient environment.

The presented measured data may be utilized to highlight cloth materials that have a reasonable (based on NIOSH guidelines) ΔP and a high FE_{min}. These data are discussed further for the best performing cloth samples; microscopic images of each are shown in Figure 6, and data are tabulated in Table 1. The top performing samples show a broad array of structure. This information plus that presented earlier reinforces the fact that visual appearance is not necessarily indicative of a fabric's filtration and pressure differential properties as previously suggested.[15] For example, the top performing cloth was Cotton 8, which had a visually loose weave, a high FE_{min} (32.0% ± 1.6%) and low ΔP (61.8 Pa ± 4.9 Pa), and a resulting QF of (6.25 ± 0.27) kPa^{-1}. In comparison, Cotton 6, which had a visually tighter weave and high yarn count (812 yarns inch^{-2}), had a lower FE_{min} (20.3 ± 1.02) % and a higher ΔP (128.5 ± 4.9) Pa, with a resulting low QF of (1.77 ± 0.04) kPa^{-1}. Another high yarn count fabric (Cotton 13, ≈ 600 yarns inch^{-2}, and the same weave type as Cotton 8) did not make this top five list and had statistically the same FE_{min} (Cotton 13 FE_{min} = 19.7% ± 1.0%) as Cotton 8 despite having ∼200 less yarns inch^{-2}.

Other 2-layered cloth materials that offer a similar combination of FE_{min} and ΔP are shown in Table 1. Using the reasonable assumption that the monotonic change in ΔP with the number of layers (e.g., Cotton 10, lightweight cotton

flannel shown in Figure 3C) is similar for other cotton materials, it can be hypothesized that the following material combinations and structures may provide the best breathability and FE_{min}: a 6-layered mask (by extrapolation from the change in ΔP observed in Figure 3C) of Cotton 8 or a 4-layered assembly of lightweight flannel (sample Cotton 10, FE_{min} = 48% and ΔP = 216 Pa). Note that these hypothesized constructions are based upon measured FE_{min} and ΔP data and do not consider the other potential guidelines that may affect mask performance such as the current WHO recommendation of utilization of mixtures of hydrophobic and hydrophilic layers[3] and the effects of mask fitment.[13]

Nonwoven, synthetic fabrics utilized in masks, such as the N95, are often constructed using a melt-bond process. Part of the goal of this process is to stabilize and compress (e.g., calendaring) the manufactured fiber-webs to enhance filtration. Similar steps to engineer the processing of natural fabrics may be necessary to improve, and help maintain, the performance of the above suggested natural fiber materials. Cloth materials with similar microscale structure could be pursued in future investigations. Comparisons between studies measuring cloth FE are challenging due to experimental parameters that may influence mask performance (e.g., sample flow rate, aerosol generation scheme, charge neutralization, and variability in protocols). Future work in this area should use established techniques and officially recognized methods such as EN 1822 or ISO standard methods. On the basis of the findings presented here, other important future research areas of cloth masks may include (1) investigating the relationship between fiber diameters, diameter ranges, and sources with FE and ΔP of select best performing fabrics, (2) an examination of the extent of napping or raised fibers on FE and ΔP and (3) the effect of washing/decontamination on FE, (4) the impact of seams, (5) the influence of relative humidity, or (6) high face velocities such as encountered during coughing or sneezing on FE.

CONCLUSION

Cloth materials considered in the construction of facemasks to reduce the transmission of SARS-CoV-2 were evaluated for key factors in mask performance: the filtration efficiency (FE), differential pressure (ΔP), and fabric construction parameters. The results indicate that there is a complex interplay between fabric type, weave, and yarn count and the filtration of nanometer-sized aerosol particles. The best performing cloth materials had moderate yarn counts with visible raised fibers. No measured cloth masks performed as well as an N95. The measured data of mixed cloth assemblies were in contrast to recent measurements by Konda et al., where mixed assemblies of multiple materials did not synergistically impact the measured FE_{min} beyond the product of individual FE values.[15] The measured data indicate that particle charge does not impact FE for both natural and synthetic fabrics.

Importantly, the presented data were measured under idealized conditions that eliminate or minimize leaks, which are important determinants in mask performance.[13] Other factors that may influence mask performance include fiber width, relative humidity, fabric moisture content, seams across the fabric, fabric nap/texture, and washing or degradation of the fabric.[60] Extending the measured particle size to mimic larger droplets will also aid in understanding fabric filtration.

The method of measuring FE using a combination of aerosol size selection and particle counting is widely available and may enable other research laboratories to perform similar measurements under controlled conditions enabling quantitative comparability of materials. The combination of microscopy and FE applied to other mask materials may allow rapid screening of a broad array of relevant materials or combinations to construct a detailed database for the optimization of FE to reduce exposure to virus-sized particles.

MATERIALS AND METHODS

Samples. Samples were acquired from multiple sources by the authors and those acknowledged. Samples were cut into a circular shape of 2.5 cm diameter using a cleaned stainless-steel form and scissors. Samples were used as received and were equilibrated at ~22 °C and at ambient relative humidity, 30% to 50%, prior to measurement. Most samples were measured in two layers, see text, and were loaded into the sample assembly as individual layers to avoid the potential of perfect registration between the two layers, which may reduce the measured FE.

The measured samples did not shed particles under the flow conditions described in this study. However, materials that meet the HEPA filtration standard may be constructed from multiple types of materials including layered polymers or glass (SiO_2) fibers. Using mask materials that meet the HEPA filter standard under conditions they were not designed for, such as cutting or the physical deformation of the filter membrane, may cause the shedding of nano- or microscale fibers from the filter increasing the likelihood of inhalation or ingestion by the mask wearer.

The fabric characterization experiments presented can be split into two sets: (1) material microscopy image analysis for fabric structure to assess material yarn count, weave, and mass measurements, and (2) the filtration efficiency of aerosolized material.

Material Imaging. Imaging was completed with an USB digital microscope (Innovation Beyond Imagination) equipped with 8 brightfield LED lights, a color CMOS sensor, and a high speed 24-bit DSP. Images were collected in diffuse reflected light (LED, ring illuminated) and transmitted light (LED lightbox, Tiktec Laboratories, using size A4 or A5). All images were calibrated to a millimeter length scale, and resolution was calculated to be ~20 μm (see Supporting Information S4 for details). Calibration was completed for each fabric type imaged. This was necessary as the differing thicknesses of the fabrics resulted in utilization of slightly different fields of view for each sample set. Preliminary processing, yarn counts, and yarn width measurements were completed in ImageJ (v. 1.8.0_112 with Fiji).[61,62] All images were length-scale calibrated and converted to an eight-bit gray scale before analyses. Additional image processing was completed in Digital Surf (Mountain Laboratories, v. 8) and was utilized to create the inverted grayscale images shown in Figure 1. Reflected and transmitted light images, yarn widths, and yarn count data can be found in SI S3.

Weave Types and Yarn Count, Width, and Mass Measurements. Reported weave types were either determined by visual inspection following the descriptions outlined in Table S38 in Section S7 of the Supporting Information or listed as described by the manufacturer. Two or more different sample sites were analyzed for each fabric for determination of yarn widths, and, unless otherwise stated, n = 20 yarns were measured. Measurements were completed manually and recorded using the measure subroutine in ImageJ. Widths were measured between yarn crossing junctions (i.e., not at the overlap of the yarns). Yarn counts were completed by measuring 1 mm across either axis of an image (starting in a void space) and then counting the number of yarns that fell under that line. Both front interior and exterior faced yarns were counted. Mean, standard deviation (reported to 1σ), minimum, and maximum values are reported for the warp and weft yarn widths (see Section S3 of the Supporting Information). Warp and weft yarn directions were utilized in this study following textile industry practices. Warp yarns are those placed on a loom before being interwoven with weft yarns (see Figure S4). Identification of these yarns was completed by either visual inspection of the selvedge or by analyzing the weave and looking for

reed marks (marks left by a tool used to separate and space yarns) in the samples.

Yarn counts were also conducted separately in the warp and weft directions. Reported yarn counts are the average results of $n = 5$ measurements across 2 or more different sample sites. In cases where there was no clear warp:weft yarn structure (e.g., knits, block, and waffle weave samples), a single value is reported for the number of yarns counted in along 1 mm of the horizontal direction of the image. Mass yarn^{-1} measurements are relative to a 1 cm^2 area and were calculated by dividing measured masses by the total number of yarns (sum of warp and weft yarns) counted for the same size area.

Filtration Efficiency. *FE* measurements mimicked Parts 3 and 5 of the EN 1822 mask filtration protocol (aerosol remains un-neutralized after size selection) or the ISO 29463 testing standard (aerosol is reneutralized after size selection); see Figure S1. Aerosol was generated from a 10 mg mL^{-1} aqueous solution of NaCl using a constant output atomizer supplied with dry (dew point < −75 °C), HEPA-filtered air (25 psig). Of the 2.2 L min^{-1} flow that was generated, 0.3 L min^{-1} was sampled and conditioned using two silica gel diffusion dryers (desiccant was replaced daily prior to data collection). The aerosol was then passed through a soft X-ray charge neutralizer and size selected, at a mobility diameter (D_m), using a differential mobility analyzer (DMA) and a 10:1 sheath:aerosol flow. Under these experimental conditions, the range of aerosols selected was 50 nm $\leq D_m \leq$ 825 nm. The ∼0.3 L min^{-1} of aerosol exiting the DMA was then mixed with ∼2.7 L min^{-1} HEPA-filtered dilution air (ambient laboratory air with ∼30% relative humidity) and either passed to a condensation particle counter (CPC) or through a 25 mm plastic filter holder (with stainless steel filter backing) to a CPC to measure the upstream (N_U) and downstream (N_D) particle number densities, respectively. Both CPCs sampled at 1.5 L min^{-1} and the face velocity at the filter holder ≈ 6.3 cm s^{-1} and in line with NIOSH guidelines. Conductive (carbon black impregnated) silicone tubing was used throughout the experiment to prevent aerosol scavenging. The material under test was held in a plastic filter holder with a polymer gasket that electrically isolated the material. No attempts were made to electrically ground the tested material.

The downstream CPC had been previously calibrated by a spectroscopic method using ammonium sulfate aerosol, see Radney and Zangmeister (2018).[40] Using this method, the CPC calibration is better than 3% for number densities (N) < 2×10^4 cm^{-3}; see additional details in the Supporting Information. At larger values of N, N_U and N_D deviated from each other, so they were compared multiple times daily using the described arrangement without fabric in the filter assembly. Both CPCs (TSI 3775) also switched between a single particle counting mode and a photometric counting mode at ∼5 × 10^4 cm^{-3}. The transition between modes was set by the manufacturer and automated based on the rate of change of N as a function of time. The transition regime of two instruments behaved similarly, but their set points may have been slightly offset under some measurement conditions. Two methods were used to account for this variation: (1) measurements with 4.5×10^4 cm^{-3} $\leq N_D \leq 5.5 \times 10^4$ cm^{-3} were excluded from the determination of the minimum *FE*, and (2) separate comparison curves between N_U and N_D were used for $N_D \geq 4.5 \times 10^4$ cm^{-3} and $N_D \leq 5.5 \times 10^4$ cm^{-3} (see Figure S2).

Experimental and data acquisition were controlled by custom software written in our laboratory. D_m (15 samples equally log spaced spanning 50 nm $\leq D_m \leq$ 825 nm) was set by a computer and the particle counts were allowed to stabilize for 30 s. The N_U and N_D were then recorded for 30 s at 1 Hz, after which the next D_m was sequentially selected. The 30 s data (representing one technical replicate) were then averaged and a 1σ standard deviation calculated. The *FE* was then calculated from eq 1 with the relative uncertainty in *FE* including the propagated 1σ uncertainties in N_U and N_D. The total time required to collect an *FE* curve for a single fabric sample was ∼15 min.

For all presented *FE* values, we assume an uncertainty of 5% that derives from (1) measured 1σ standard deviations of $N \approx 2.5\%$, (2) CPC accuracy ≈ 3% (we assume this is constant for all N and not just $N < 2 \times 10^4$ cm^{-3}), (3) an ∼2% day-to-day variability in *FE* for the

same sample, and (D) ∼1% sample-to-sample variability in *FE* for the same material.

The calculated *FE* curves were then converted to penetration efficiency (*PE* = 100% − *FE*) and fit as a function of D_m to a logarithmic bi-Gaussian distribution (*i.e.*, a logarithmically trans-formed bi-Gaussian distribution):

$$PE = \begin{cases} PE_{max} \times \exp\left(\dfrac{-(\log_{10}(D) - \log_{10}(D_{ae}))^2}{2(\log_{10}\sigma_1)^2} \right) & D \leq D_m \\[4mm] PE_{max} \times \exp\left(\dfrac{-(\log_{10}(D) - \log_{10}(D_{ae}))^2}{2(\log_{10}\sigma_2)^2} \right) & D > D_m \end{cases} \quad (3)$$

where PE_{max} is the maximum penetration efficiency of the material. To be consistent with other reports, we report all data as the filtration efficiency (*FE*) as shown in eq 1.

The differential pressure (ΔP, Pa) across the filter sample was measured using one of two manometers with ranges of 0 to 245.17 Pa and 0 to 490.3 Pa; to convert from Pa to mm H$_2$O to Pa, divide by 9.80665 Pa.[63] The reported ΔP across the filter represents the difference between the filter assembly with and without a filter present. Uncertainty in ΔP was calculated as twice the manometer read error (±4.9 Pa, 1σ).

Outlier and Correlation Calculations. The 100% cotton ($n = 11$) and 100% polyester ($n = 5$) sample sets were selected for correlation calculations by controlling for fiber type (cotton or polyester) and utilizing data sets on fabrics only with definite yarn counts. The data sets consisted of the following parameters: FE_{min} (%), ΔP (mm H$_2$O), weft and warp yarn widths (mm), weft and warp yarn counts (yarn inch^{-1}), yarn count (yarns inch^{-2}), and areal yarn mass (mg yarn^{-1}). Parameter outliers were determined by calculating the first (25%) and third (75%) quartiles, determining the interquartile range from these values, calculating the upper and lower bounds of the range, and then rejecting any data value that fell outside of these bounds. Results from these calculations along with other descriptive statistical values for each parameter analyzed are presented in Tables S34 and S35 in Section S5 of the Supporting Information.

The remaining data were tested for normal distribution using the Shapiro-Wilk Test for Normality.[64] Normality test results were employed to determine whether to use a parametric (Pearson Product Moment Correlation, normally distributed data sets, eq 4) or a nonparametric (Spearman Rank-Order Correlation, non-normally distributed data sets, eq 5) correlation equation on pairs of data sets:

$$r_p = \frac{n\left(\sum x_i y_i\right) - \left(\sum x_i\right)\left(\sum y_i\right)}{\sqrt{\left[n\sum x_i^2 - \left(\sum x_i\right)^2\right]\left[n\sum y_i^2 - \left(\sum y_i\right)^2\right]}} \quad (4)$$

$$r_s = \frac{6\sum (rg(x_i) - (rg(y_i))^2}{n(n^2 - 1)} \quad (5)$$

where x_i and y_i are raw values for the *i*th set, n is the number of observations, and $rg(x_i)$ and $rg(y_i)$ are converted ranks for defined values.

These tests were selected under the assumptions that (1) variables are independent, (2) the values in the nonparametric sets are interval variables, and (3) there is a monotopic relationship between variables. Paired sets where both data sets failed the Shapiro-Wilk test and paired sets where only one failed the Shapiro-Wilk test were treated with the Spearman test, and the Pearson test was only utilized with pairs that both tested positive for normality. Pearson coefficients (r_p), and Spearman coefficients (r_s), and their corresponding *p*-values (ρ_p and ρ_s, respectively) were calculated in SigmaPlot (version 14).[65] Results are reported in Tables S36 and S37 in Section S5 of the Supporting Information. Calculated coefficients were evaluated for significance based on the following criteria: variables with *p*-values below 0.050 and positive (+) coefficients tend to increase together;

pairs with *p*-values below 0.050 and negative coefficients (−) have one variable that tends to decrease while the other increases. There is no significant relationship between two variables for pairs where the *p*-values are greater than 0.050.[65] Presented correlation results should be interpreted cautiously given the small number of observations in this study per the controlled population sizes.

ASSOCIATED CONTENT

Ⓢ Supporting Information

The Supporting Information is available free of charge at https://pubs.acs.org/doi/10.1021/acsnano.0c05025.

FE measurement description and schematic, measurements of particle counts for N_U and N_D and *FE* as function of D_m, description of method of image analysis, microscopic images, yarn widths, number of yarns in weft and warp directions, number of yarns cm^{-2} for each measured sample (PDF)

AUTHOR INFORMATION

Corresponding Author

Christopher D. Zangmeister − *Material Measurement Laboratory, National Institute of Standards and Technology, Gaithersburg, Maryland 20899, United States;* ⦿ orcid.org/0000-0002-6026-9293; Phone: (301) 975-8709; Email: cdzang@nist.gov

Authors

James G. Radney − *Material Measurement Laboratory, National Institute of Standards and Technology, Gaithersburg, Maryland 20899, United States;* ⦿ orcid.org/0000-0001-7324-8769

Edward P. Vicenzi − *Museum Conservation Institute, Smithsonian Institution, Suitland, Maryland 20746, United States; Material Measurement Laboratory, National Institute of Standards and Technology, Gaithersburg, Maryland 20899, United States*

Jamie L. Weaver − *Material Measurement Laboratory, National Institute of Standards and Technology, Gaithersburg, Maryland 20899, United States; Museum Conservation Institute, Smithsonian Institution, Suitland, Maryland 20746, United States;* ⦿ orcid.org/0000-0002-6762-0568

Complete contact information is available at:
https://pubs.acs.org/10.1021/acsnano.0c05025

Author Contributions

§Second affiliations are via nonfunded, guest research appointments at listed institutions.

Notes

Trade names and commercial products are identified in this paper to specify the experimental procedures in adequate detail. This identification does not imply recommendation or endorsement by the authors or by the National Institute of Standards and Technology, nor does it imply that the products identified are necessarily the best available for the purpose. The authors declare no competing financial interest.

REFERENCES

(1) Health Emergencies Preparedness and Response Team. *Advice on the Use of Masks in the Context of COVID-19: Interim Guidance, 6 April 2020, 2020. Advice on the Use of Masks in the Context of COVID-19: Interim Guidance;* WHO, 2020. https://apps.who.int/iris/handle/10665/331693 (accessed 06-23-2020).

(2) United States Centers for Disease Control and Prevention. *Coronavirus Disease 2019 (COVID-2019);* CDC, 2020. https://www.cdc.gov/coronavirus/ (accessed 06-23-2020).

(3) Health Emergencies Preparedness and Response Team. *Advice on the Use of Masks in the Context of COVID-19: Interim Guidance, 5 June 2020;* WHO, 2020. https://www.who.int/publications/i/item/advice-on-the-use-of-masks-the-community-during-home-care-and-in-health-care-settings-in-the-context-of-the-novel-coronavirus-(2019-ncov)-outbreak (accessed 06-23-2020).

(4) Neuman, B.; Adair, B.; Yoshioka, C.; Quispe, J.; Orca, G.; Kuhn, P.; Milligan, R.; Yeager, M.; Buchmeier, M. Supramolecular Architecture of Severe Acute Respiratory Syndrome Coronavirus Revealed by Electron Cryomicroscopy. *J. Virol.* **2006**, *80*, 7918−7928.

(5) Liu, Y.; Ning, Z.; Chen, Y.; Guo, M.; Liu, Y.; Gali, N. K.; Sun, L.; Duan, Y.; Cai, J.; Westerdahl, D.; Liu, X.; Xu, K.; Ho, K.; Kan, H.; Fu, Q.; Lan, K. Aerodynamic Analysis of SARS-COV-2 in Two Wuhan Hospitals. *Nature* **2020**, *582*, 557−560.

(6) Prather, K.; Wang, C.; Schooley, R. Reducing Transmission of SARS-COV-2. *Science* **2020**, *368*, 1422−1424.

(7) Milton, D.; Fabian, M.; Angel, M.; Perez, D.; Mcdevitt, J. Influenza Virus Aerosols in Human Exhaled Breath: Particle Size, Culturability, and Effect of Surgical Masks. *PLoS Pathog.* **2010**, *9*, No. e1003205.

(8) Weaver, G. Droplet Infection and Its Prevention by the Face Mask. *J. Infect. Dis.* **1919**, *24*, 218−230.

(9) Kellogg, W.; Macmillan, G. An Experimental Study of the Efficacy of Gauze Face Masks. *Am. J. Public Health* **1920**, *10*, 34−42.

(10) Rengasamy, S.; Eimer, B.; Shaffer, R. Simple Respiratory Protection-Evaluation of the Filtration Performance of Cloth Masks and Common Fabric Materials against 20−1000 nm Size Particles. *Ann. Occup. Hyg.* **2010**, *54*, 789−798.

(11) Shakya, K.; Noyes, A.; Kallin, R.; Peltier, R. Evaluating the Efficacy of Cloth Facemasks in Reducing Particulate Matter Exposure. *J. Exposure Sci. Environ. Epidemiol.* **2017**, *27*, 352−357.

(12) Davies, A.; Thompson, K.; Giri, K.; Kafatos, G.; Walker, J.; Bennett, A. Testing the Efficacy of Homemade Masks: Would They Protect in an Influenza Pandemic? *Disaster Med. Public Health Prep* **2013**, *7*, 413−418.

(13) Lai, A.; Poon, C.; Cheung, A. Effectiveness of Facemasks to Reduce Exposure Hazards for Airborne Infections among General Populations. *J. R. Soc., Interface* **2012**, *9*, 938−948.

(14) Van Der Sande, M.; Teunis, P.; Sabel, R. Professional and Home-Made Face Masks Reduce Exposure to Respiratory Infections among the General Population. *PLoS One* **2008**, *3*, No. e2618.

(15) Konda, A.; Prakash, A.; Moss, G.; Schmoldt, M.; Grant, G.; Guha, S. Aerosol Filtration Efficiency of Common Fabrics Used in Respiratory Cloth Masks. *ACS Nano* **2020**, *14*, 6339−6347.

(16) Macintyre, C.; Seale, H.; Dung, T.; Hien, N.; Nga, P.; Chughtai, A.; Rahman, B.; Dwyer, D.; Wang, Q. A Cluster Randomised Trial of Cloth Masks Compared with Medical Masks in Healthcare Workers. *Bmj Open* **2015**, *5*, No. e006577.

(17) Kulkarni, P.; Baron, P.; Willeke, K. *Aerosol Measurement: Principles, Techniques and Applications*. 3rd ed.; John Wiley & Sons, Inc.: Hoboken, NJ, 2011; 107−128.

(18) Brown, R.; Wake, D. Air Filtration by Interception—Theory and Experiment. *J. Aerosol Sci.* **1991**, *22*, 181−186.

(19) Emi, H.; Okuyama, K.; Yoshioka, N. Prediction of Collection Efficiency of Aerosols by High-Porosity Fibrous Filter. *J. Chem. Eng. Jpn.* **1973**, *6*, 349−354.

(20) Stechkina, I.; Fuchs, N. Studies on Fibrous Aerosol Filters-I. Calculation of Diffusional Deposition of Aerosols in Fibrous Filters. *Ann. Occup. Hyg.* **1966**, *9*, 59−64.

(21) Stechkina, I.; Kirsch, A.; Fuchs, N. Studies on Fibrous Aerosol Filters-IV Calculation of Aerosol Deposition in Model Filters In the Range of Maximum Penetration. *Ann. Occup. Hyg.* **1969**, *12*, 1−8.

(22) Lee, K.; Liu, B. Theoretical Study of Aerosol Filtration by Fibrous Filters. *Aerosol Sci. Technol.* **1982**, *1*, 147−161.

(23) Podgórski, A.; Bałazy, A.; Gradoń, L. Application of Nanofibers to Improve the Filtration Efficiency of the Most Penetrating Aerosol Particles in Fibrous Filters. *Chem. Eng. Sci.* **2006**, *61*, 6804−6815.

(24) *Specification for HEPA Filters Used by DOE Contractors; DOE-STD-3020−2015*; U. S. Department of Energy: Washington, D.C., 2015; pp 1−29.

(25) Hinds, W. C. *Aerosol Technology: Properties, Behavior, and Measurement of Airborne Particles*, 2nd ed.; John Wiley & Sons, Inc.: New York, 1999; pp 182−205.

(26) Rengasamy, S.; Shaffer, R.; Williams, B.; Smit, S. A Comparison of Facemask and Respirator Filtration Test Methods. *J. Occup. Environ. Hyg.* **2017**, *14*, 92−103.

(27) *Determination of Particulate Filter Efficiency Level for N95 Series Filters Against Solid Particulates for Non-Powdered, Air-Purifying Respirators Standard Testing Procedure (STP); TEB-APR-STP-0059*; National Institute for Occupational Safety and Health: Pittsburgh, PA, 2019; pp 1−9.

(28) Leung, N.; Chu, D.; Shiu, E.; Chan, K.; Mcdevitt, J.; Hau, B.; Yen, H.; Li, Y.; Ip, D.; Peiris, J.; Seto, W.; Leung, G.; Milton, D.; Cowling, B. Respiratory Virus Shedding in Exhaled Breath and Efficacy of Face Masks. *Nat. Med. (N. Y., NY, U. S.)* **2020**, *26*, 676−680.

(29) Schiefer, H.; Taft, D.; Porter, J. Effect of Number of Warp and Filling Yarns per Inch and Some Other Elements of Construction on the Properties of Cloth. *J. Res. Natl. Bur. Stand.* **1936**, *16*, 139−147.

(30) Mainelis, G.; Willeke, K.; Baron, P.; Grinshpun, S.; Reponen, T. Induction Charging and Electrostatic Classification of Micrometer-Size Particles for Investigating the Electrobiological Properties of Airborne Microorganisms. *Aerosol Sci. Technol.* **2002**, *36*, 479−491.

(31) Willeke, K.; Whitby, K. Atmospheric Aerosols: Size Distribution Interpretation. *J. Air Pollut. Control Assoc.* **1975**, *25*, 529−534.

(32) Chen, C.; Huang, S. The Effects of Particle Charge on the Performance of a Filtering Facepiece. *Am. Ind. Hyg. Assoc. J.* **1998**, *59*, 227−233.

(33) Kowalski, W.; Bahnfleth, W.; Whittam, T. Filtration of Airborne Microorganisms: Modeling and Prediction. In *AHRAE Transactions, Seattle WA, 06/18/1999−06/23/1999*; Geshwiler, M., Harrell, D., Roberson, T., Eds.; American Society of Heating, Refrigerating and Air-Conditioning Engineers, Inc.: Seattle, WA, 1999; Vol. *4273*, pp 4−17.

(34) Zhou, S.; Lukula, S.; Chiossone, C.; Nims, R.; Suchmann, D.; Ijaz, M. Assessment of a Respiratory Face Mask for Capturing Air Pollutants and Pathogens Including Human Influenza and Rhinoviruses. *J. Thorac. Dis.* **2018**, *10*, 2059−2069.

(35) Lee, S.; Obendorf, S. Statistical Model of Pesticide Penetration through Woven Work Clothing Fabrics. *Arch. Environ. Contam. Toxicol.* **2005**, *49*, 266−273.

(36) Zhao, M.; Liao, L.; Xiao, W.; Yu, X.; Wang, H.; Wang, Q.; Lin, Y.; Kilinc-Balci, F.; Price, A.; Chu, L.; Chu, M.; Chu, S.; Cui, Y. Household Materials Selection for Homemade Cloth Face Coverings and Their Filtration Efficiency Enhancement with Triboelectric Charging. *Nano Lett.*. **2020**. DOI: 10.1021/acs.nanolett.0c02211.

(37) Alekseeva, L. Theoretical Aspects of Predicting the Electrostatic Properties of Textile Materials. *Fibre Chem.* **2007**, *39*, 225−226.

(38) Žilinskas, P.; Lozovski, T.; Jankauskas, V.; Jurksus, J. Electrostatic Properties and Characterization of Textile Materials Affected by Ion Flux. *Mater. Sci.-Polym.* **2013**, *19*, 61−66.

(39) Kadolph, S.; Marcketti, S. *Textiles*, 12th ed.; Pearson: Boston, MA, 2016; pp 164−165.

(40) Radney, J.; Zangmeister, C. Comparing Aerosol Refractive Indices Retrieved from Full Distribution and Size- and Mass-Selected Measurements. *J. Quant. Spectrosc. Radiat. Transfer* **2018**, *220*, 52−66.

(41) Wiedensohler, A. An Approximation of the Bipolar Charge Distribution for Particles in the Submicron Size Range. *J. Aerosol Sci.* **1988**, *19*, 387−389.

(42) Radney, J.; Ma, X.; Gillis, K.; Zachariah, M.; Hodges, J.; Zangmeister, C. Direct Measurements of Mass-Specific Optical Cross Sections of Single Component Aerosol Mixtures. *Anal. Chem.* **2013**, *85*, 8319−8325.

(43) Radney, J.; Zangmeister, C. Practical Limitations of Aerosol Separation by a Tandem Differential Mobility Analyzer−Aerosol Particle Mass Analyzer. *Aerosol Sci. Technol.* **2016**, *50*, 160−172.

(44) Buys, T.; De Clerk, K. Bi-Gaussian Fitting of Skewed Peaks. *Anal. Chem.* **1972**, *44*, 1273−1275.

(45) *Determination of Inhalation Resistance TEB-APR-STP-0007*; National Institute for Occupational Safety and Health: Pittsburgh, PA, 2019; pp 1−7.

(46) *Determination of Exhalation Resistance TEB-APR-STP-0003*; National Institute for Occupational Safety and Health: Pittsburgh, PA, 2019; pp 1−6.

(47) Chen, C.; Willeke, K. Aerosol Penetration through Surgical Masks. *Am. J. Infect. Control* **1992**, *20*, 177−184.

(48) *Food and Drugs; Sterilization Wrap, 21CFR880.6850*; Food and Drug Administration: Silver Spring, MD, 2020.

(49) Chattopadhyay, S.; Hatton, T.; Rutledge, G. Aerosol Filtration Using Electrospun Cellulose Acetate Fibers. *J. Mater. Sci.* **2016**, *51*, 204−217.

(50) Payen, J.; Vroman, P.; Lewandowski, M.; Perwuelz, A.; Callé-Chazelet, S.; Thomas, D. Influence of Fiber Diameter, Fiber Combinations and Solid Volume Fraction on Air Filtration Properties in Nonwovens. *Text. Res. J.* **2012**, *82*, 1948−1959.

(51) Hosseini, S.; Tafreshi, H. On the Importance of Fibers' Cross-Sectional Shape for Air Filters Operating in the Slip Flow Regime. *Powder Technol.* **2011**, *212*, 425−431.

(52) Bradow, J.; Davidonis, G. Quantitation of Fiber Quality and the Cotton Production-Processing Interface: A Physiologist's Perspective. *J. Cotton Sci.* **2000**, *4*, 34−64.

(53) Bailey, B. Diameter Relationships of Wool Fibers from Five Breeds of Sheep Raised in South Dakota. *J. Agric. Res.* **1940**, *60*, 415−426.

(54) Stobart, R.; Russell, W.; Larsen, S.; Johnson, C.; Kinnison, J. Sources of Variation in Wool Fiber Diameter. *J. Anim. Sci.* **1986**, *62*, 1181−1186.

(55) American Sheep Industry Association. *Sheep Production Handbook*; Sheep Industry Development Program, 1988; wool-13−wool-73.

(56) Grafe, T.; Graham, K. Polymeric Nanofibers and Nanofiber Webs: A New Class of Nonwovens. *Int. Nonwovens J.* **2003**, *os-12*, 51−55.

(57) Brown, P.; Cox, C. *Fibrous Filter Media*; Elsevier: Cambridge, MA, 2017; pp 51−94.

(58) Perumalraj, R. Characterization of Electrostatic Discharge Properties of Woven Fabrics. *J. Text. Sci. Eng.* **2015**, *6*, 1−6.

(59) Forsyth, B.; Liu, B.; Romay, F. Particle Charge Distribution Measurement for Commonly Generated Laboratory Aerosols. *Aerosol Sci. Technol.* **1998**, *28*, 489−501.

(60) Pusic, T.; Grancaric, A.; Soljacic, I.; Ribitsch, V. The Effect of Mercerisation on the Electrokinetic Potential of Cotton. *Color. Technol.* **1999**, *115*, 121−124.

(61) Schindelin, J.; Arganda-Carreras, I.; Frise, E.; Kaynig, V.; Longair, M.; Pietzsch, T.; Preibisch, S.; Rueden, C.; Saalfeld, S.;

Schmid, B.; Tinevez, J.; White, D.; Hartenstein, V.; Eliceiri, K.; Tomancak, P.; Cardona, A. Fiji: An Open-Source Platform for Biological-Image Analysis. *Nat. Methods* **2012**, *9*, 676−682.

(62) Rueden, C.; Schindelin, J.; Hiner, M.; Dezonia, B.; Walter, A.; Arena, E.; Eliceiri, K. ImageJ2: ImageJ for the Next Generation of Scientific Image Data. *BMC Bioinf.* **2017**, *18*, 1−26.

(63) Thompson, A.; Taylor, B. *Guide for the Use of the International System of Units (SI) 811*; National Institute of Standards and Technology: Gaithersburg, MD, 2008; p 90.

(64) Shapiro, S.; Wilk, M. An Analysis of Variance Test for Normality (Complete Samples). *Biometrika* **1965**, *52*, 591−611.

(65) Bertrand, C. Graphing Wizardry. *Science* **2000**, *289*, 1893−1894.